Available online at www.sciencedirect.com

ScienceDirect

Russian Geology and Geophysics 55 (2014) 89–97

RUSSIAN GEOLOGY AND GEOPHYSICS

www.elsevier.com/locate/rgg

Approximation of a near-vertical boundary in the problems of pulsed electromagnetic soundings

N.V. Shtabel' [a,*], M.I. Epov [a,b], E.Yu. Antonov [a], M.A. Korsakov [a]

[a] *A.A. Trofimuk Institute of Petroleum Geology and Geophysics, Siberian Branch of the Russian Academy of Sciences, pr. Akademika Koptyuga 3, Novosibirsk, 630090, Russia*

[b] *Novosibirsk State University, ul. Pirogova 2, Novosibirsk, 630090, Russia*

Received 19 December 2012; accepted 23 May 2013

Abstract

We analyze the results of a mathematical simulation of pulsed electromagnetic fields in geologic media with dipping near-vertical boundaries as well as interpretations within approximating block models and a layered homogeneous conducting model. We consider the possibilities and limitations of these approaches to the inversion of data from pulsed soundings of actual geologic media.

Keywords: vector finite-element method; 3D modeling; pulsed electromagnetic soundings

Introduction and problem formulation

The theory of nonstationary soundings is based on analysis of the spatial distribution of the electromagnetic field in horizontally layered models for conducting nonmagnetic isotropic geologic media. The most widespread ground unit consists of several closed circuits (coils): one transmitter and receivers.

When current within the circuit is switched off, ring eddy current develops beneath the surface of the conducting half-space, according to Faraday's induction law. The electromagnetic field is formed by secondary eddy currents induced in the conducting parts of the medium.

Eddy currents make up moving toroid structures, often called "smoke rings." Some time after the switch-off, the eddy current toroid dips into the medium and its radius and cross-section increase. In the conducting half-space, the toroid center moves along a straight path inclined at ~28° to its surface (Epov et al., 1994; Nabighian, 1979). If a horizontally layered model is based on an insulator, its path levels out and it begins to move horizontally with time (so-called S zone). In this case, the electric field does not cross the inner boundaries, at which conductivity changes in a saltatory manner.

The described process degenerate in terms of the generation of the secondary electromagnetic field, because sources of the second type (charges) do not participate therein. They appear in the medium in the presence of nonhorizontal boundaries. The eddy electric field crosses the inner boundaries, on whose surface charges appear with a density proportional to the average normal component of the electric field at the boundary. The proportionality coefficient is called "the contrast coefficient" and described by the simple expression

$$k_{12} = \frac{\sigma_+ - \sigma_-}{\sigma_+ + \sigma_-},$$

where σ_+, σ_- are the conductivities of the medium at both sides of the boundary.

Importantly, the surface charges are confined to the boundaries and can move only along them. On the other hand, the eddy current toroid moves within the entire half-space over time. In this case, the eddy currents and surface charges interact, especially if there are several dipping boundaries in the medium. The conventional division of the field into two modes—induction (eddy currents) and galvanic (charges)—loses its physical meaning and cannot be used to the full when the behavior of the nonstationary electromagnetic field is analyzed.

Present-day systems of 3D inversion are usually based on a class of models consisting of a set of conducting areas, which are separated by a system of horizontal and vertical bounda-

* Corresponding author.
E-mail address: nadino2000@mail.ru (N.V. Shtabel')

1068-7971/$ - see front matter © 2014, V.S. Sobolev IGM, Siberian Branch of the RAS. Published by Elsevier B.V. All rights reserved.
http://dx.doi.org/10.1016/j.rgg.2013.12.007

ries. Such a description of the medium leaves open the question of measured-signal inversion in widespread cases, when dipping boundaries are present. How adequate the approximation of the dipping boundary by a set of horizontal and vertical planes is, remains unclear. If their number is large, it is evident from physical considerations that the values of nonstationary electromagnetic fields in these two models will approach one another. If the number of the approximating horizontal and vertical plane boundaries is small, the distribution of surface charges at the dipping boundary will differ considerably. It is continuous at the dipping boundary, and the density at the horizontal boundaries will change in a saltatory manner.

Forward mathematical modeling is used in this study to assess the possibility of describing dipping boundaries by simpler models with horizontal and vertical boundaries.

For simplicity, we consider a model with one dipping (40º) plane separating two areas of different conductivities. It will be approximated by a stepwise set of vertical and horizontal surfaces. The number and sizes of the steps necessary for the approximation of the dipping boundary will be defined so that the nonstationary fields on the surface of the half-space will differ by no more than 1–3%. The behavior of the nonstationary electromagnetic field will be analyzed in more complicated models with several dipping boundaries. Finally, the consequences of model inconsistency in the inversion of such signals within horizontally layered models will be considered.

Models for the medium and sounding unit

The model is a parallelepiped measuring $3 \times 3 \times 4$ km and divided into two subareas: almost nonconducting (air) and conducting (ground), each 2 km high. We presume that the medium is nonmagnetic and nonpolarizing ($\mu = \mu_0 = 4\pi \times 10^7$ H/m, $\varepsilon = \varepsilon_0 = 8.854 \times 10^{-12}$ F/m). The air resistivity is taken equal to 10^6 Ohm·m. The sounding unit, located on the surface of the conducting medium, consists of coaxial square coils (transmitter, 100×100 m; receiver, 25×25 m).

Cartesian coordinates *xyz* are introduced. Their origin coincides with the center of the transmitter coil. The day surface is described by the equation $z = 0$. The inner boundaries are tilted with respect to the day surface. The tilt angles of the boundaries on the vertical plane $x0z$ will be designated by θ.

Model 1 (Fig 1*a*). The conducting area is divided by a dipping plane crossing the day surface at a distance of 500 m from the unit center at $\theta = 40º$. The subarea to the right of the dipping boundary has a resistivity of 200 Ohm·m, whereas that to the left, 10 Ohm·m.

Models 2 and 3 (Fig. 1*b*, *c*) have the same structure but different resistivities. Model 2 has two dipping boundaries. The main boundary *1* is tilted at $\theta = 40°$ (as in model 1) and perpendicular to the additional boundary *2*. The intersection of the dipping boundaries in model 3 is localized 500 m to depth from the unit center. The depth of the intersection of the dipping planes in model 4 is 100 m. The resistivities of the subareas to the right and to the left of boundary *1* are 200 and 10 Ohm·m. The area bounded by the dipping planes in models 2 and 3 might be conducting (resistivity 5 Ohm·m) or nonconducting (resistivity 1000 Ohm·m).

Model 4 (Fig. 1*d*). The conducting area is divided into layers by three horizontal boundaries ($z = 250$, 500, and 750 m). The dipping boundary crosses them at $\theta = 40º$. The upper layer (250 m thick) to the right of the dipping boundary is characterized by two resistivity values: 5 and 1000 Ohm·m. The second layer has a resistivity of 200 Ohm·m, and the underlying layer, 10 Ohm·m.

The modeled signal is nonstationary electromotive force (EMF) observed in the receiver coil after switching off the generator. Recording time, up to 10 ms.

Mathematical simulation

As the studied model is essentially three-dimensional, the simulation method should be selected with regard to the dimensions and configuration of the sounding unit as well as the structure of the area. The method should take into account the influence of boundaries with very contrasting conductivities. The above requirements are fulfilled by the vector finite-element method (VFEM). Tetrahedral elements are used in the triangulation, because they permit "condensing" the grid near the sounding unit (coil–coil) and/or other small elements of the medium. The solution of the forward problem is the EMF induced in the receiver circuit depending on time after switching off the current pulse in the transmitter coil.

The electric field in the quasi-stationary approximation, which appears in the medium after switching off the transmitter current, is described by the corollary of Maxwell's equations

$$\begin{gathered} \operatorname{rot} \mu^{-1} \operatorname{rot} \mathbf{E} + \sigma \frac{\partial \mathbf{E}}{\partial t} = -\frac{\partial \mathbf{J}^0}{\partial t}, \\ \mathbf{E} \times \mathbf{n}\,|_{\partial\Omega} = 0, \quad \mathbf{E}\,|_{t=0} = 0, \end{gathered} \tag{1}$$

where $\mathbf{E}$ is the vector of the electric-field intensity; $\mathbf{J}^0$, vector of the extrinsic-current density in the transmitter vs. time; μ, magnetic permeability; σ, conductivity of the medium; and $\partial\Omega$, outer boundaries.

Let us introduce the functional spaces in which the solution of (1) will be searched for:

$$H(\mathrm{rot}, \Omega) = \left\{ \mathbf{u} \in L^2(\Omega) \mid \nabla \times \mathbf{u} \in L^2(\Omega) \right\},$$

$$H_0(\mathrm{rot}, \Omega) = \left\{ \mathbf{u} \in H(\mathrm{rot}, \Omega) \mid \mathbf{u} \times \mathbf{n}|_{\partial\Omega} = 0 \right\}.$$

With the corresponding scalar product and norms,

$$(\mathbf{u}, \mathbf{v})_\Omega = \int_\Omega \mathbf{u} \cdot \mathbf{v}\, dx, \quad \|\mathbf{u}\| = \sqrt{(\mathbf{u}, \mathbf{u})_\Omega},$$

$$\|\mathbf{u}\|^2_{H(\mathrm{rot}, \Omega)} = \|\mathbf{u}\|^2_\Omega + \|\nabla \times \mathbf{u}\|^2_\Omega .$$

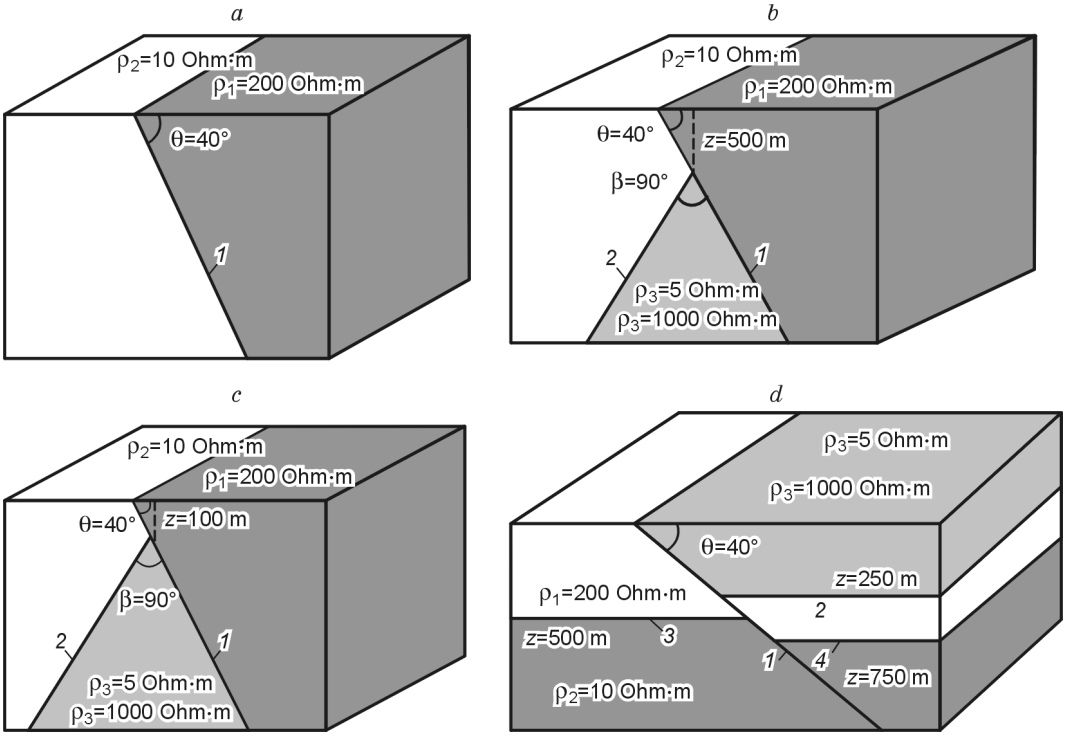

Fig. 1. Geometry of the computational domains. *a–d*, See description in the text. *1–4*, boundaries.

Let us carry out a variational formulation of the problem: to find $\mathbf{E} \in H_0(\mathrm{rot}, \Omega) \times (0, T)$ for given $\mathbf{J} \in L^2(\Omega) \times (0, T)$, so that $\forall \mathbf{W} \in H_0(\mathrm{rot}, \Omega) \times (0, T)$ is fulfilled

$$(\mu^{-1} \mathrm{rot}\, \mathbf{E}, \mathrm{rot}\, \mathbf{W})_\Omega + \sigma \left(\frac{\partial \mathbf{E}}{\partial t}, \mathbf{W} \right)_\Omega =$$

$$- \left(\frac{\partial \mathbf{J}}{\partial t}, \mathbf{W} \right)_\Omega - \int_\Omega \mu^{-1} (\mathbf{W} \times \mathbf{n}) \mathrm{rot}\, \mathbf{E}\, dS. \quad (2)$$

The finite-dimensional solution E^h, which satisfies (2), is an expansion in basic functions associated with triangulation elements:

$$\mathbf{E}^h(x, t) = \sum_{i=1}^{N} e_i(t)\, \mathbf{W}_i(x),\ \mathbf{W}_i \in H^h(\mathrm{rot}, \Omega),$$

where $\mathbf{W}_i$ indicates elements of the discrete subspace $H^h(\mathrm{rot}, \Omega)$, defined as

$$H^h(\mathrm{rot}, \Omega) = \mathrm{span}\left\{ \mathbf{W}_1, \mathbf{W}_2, ..., \mathbf{W}_n \right\} \subset H_0(\mathrm{rot}, \Omega).$$

Since the simulation method is the VFEM, Nédélec's vector edge functions of the first order, associated with the edges of the tetrahedral division (Nédélec, 1980), are selected to be the $\mathbf{W}_i$ basic functions. The use of the edge basis permits automatic fulfilment of the conditions of the continuity of the electric-field tangential components at the boundaries directly in the variational formulation (Nédélec, 1986).

At the outer boundaries of the simulation domain, the electric-field tangential component is taken equal to zero: $\mathbf{E} \times \mathbf{n}|_{\partial\Omega} = 0$ (Tamm, 1976). The size of the area is determined from the distance between the outer boundary and the unit. It should be no less than 15 sizes of the transmitter coil on the horizontal plane, whereas the EMF attenuation should be no less than 200 dB.

With regard to the expansion and boundary conditions, the discrete analog of the variational formulation will take the following form:

to find $\mathbf{E}^h \in H^h(\mathrm{rot}, \Omega) \times (0, T)$ for $\mathbf{J} \in L^2(\Omega) \times (0, T)$, so that the equation

$$(\mu^{-1} \mathrm{rot}\, \mathbf{E}^h, \mathrm{rot}\, \mathbf{W}^h)_\Omega + \sigma \left(\frac{\partial \mathbf{E}^h}{\partial t}, \mathbf{W}^h \right)_\Omega = - \left(\frac{\partial \mathbf{J}}{\partial t}, \mathbf{W}^h \right)_\Omega$$

is fulfilled for $\forall \mathbf{W}^h \in H^h(\mathrm{rot}, \Omega) \times (0, T)$.

In matrix form, it looks like

$$A\mathbf{e} + \sigma C \frac{\partial \mathbf{e}}{\partial t} = - \frac{\partial \mathbf{F}}{\partial t},$$

where

$$[A]_{ij} = \int_\Omega \mu^{-1} \mathrm{rot}\, \mathbf{W}_i \cdot \mathrm{rot}\, \mathbf{W}_j\, d\Omega, \quad i, j = 1, N_e,$$

$$[C]_{ij} = \int_\Omega \mathbf{W}_i \cdot \mathbf{W}_j\, d\Omega, \quad i, j = 1, N_e,$$

$$[F]_i = \int_\Omega \mathbf{J}^0 \cdot \mathbf{W}_i\, d\Omega, \quad i, j = 1, N_e,$$

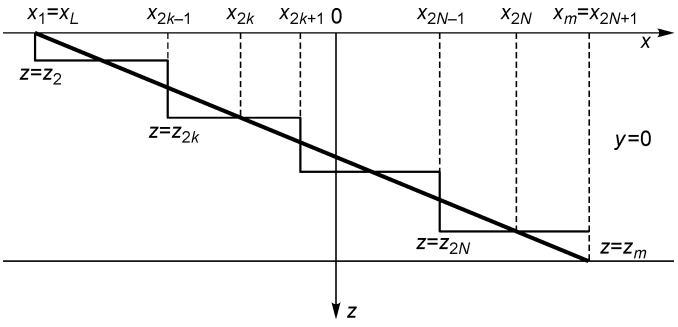

Fig. 2. Stepwise approximation of the dipping boundary.

A program modeling the nonstationary electromagnetic field in an inhomogeneous conducting medium was developed in C++ by the above algorithms (Epov et al., 2012).

Uniform piecewise constant approximation of the dipping plane boundary

The equation for the dipping-boundary intersection with any vertical plane, x = const, can be written as

$$z = -x \tan\theta + H \text{ or } x = (H - z)\cot\theta,$$

where H is the dipping-boundary depth beneath the transmitter-coil center.

The dipping boundary reaches the surface ($z = 0$) and base ($z = z_m$) on the lines (at any y)

$$x_L = H\cot\theta, \quad x_m = x_L + z_m\cot\theta.$$

In Fig. 2, the dipping boundary is approximated on the vertical plane by a set of vertical and horizontal segments. The interval $\{x = x_1 = x_L,\ x = x_{2N+1} = x_m\}$ is split into an even number of $2N$ segments. The horizontal-segment depth within the interval (x_{2k-1}, x_{2k+1}) equals the dipping-boundary depth at the even-numbered point x_{2k}: $z_{2k} = x_{2k}\cot\theta$.

For comparison, a set of models will be used with a number of pairs of vertical and horizontal segments proportional to the power of 2 ($M = 2N = 4$, 8, 16, 32, 64). The transient process $\varepsilon(t)$ in a model with a dipping boundary is selected as a reference.

Table 1. Parametrization of the stepwise model

Number of expansions	Vertical segment, m	Horizontal segment, m
2	840	100
4	420	500
8	210	250
16	105	125
32	52.5	62.5
64	26.25	31.25

The lengths of the approximating segments are shown in Table 1.

All the calculations of the EMF $\tilde{\varepsilon}(t)$ for models with an approximated boundary are compared with the EMF $\varepsilon(t)$ in the reference model.

Table 2 shows the maximum values of $\delta\varepsilon_N$ deviations in the approximated models at different numbers of M expansions with respect to $\varepsilon(t)$ signals in the reference model. Changes in the relative mistiming after switching off the transmitter current are shown in Fig. 3.

The approximation of the boundary with the minimum number of expansions (M = 2, 4) causes considerable EMF deviations from the reference model. With increasing number of expansions, the relative differences are 11% (M = 8) and 4% (M = 16). At M = 32, the difference is no more than 1.4%. In this case, the reference curve $\varepsilon(t)$ can be regarded as approximated with sufficient accuracy. Thus, the approximation of a dipping boundary by a set of stepwise boundaries requires a detailed expansion, so that the thickness of the skin layer is close to the length of the approximating segments.

Sources of the electromagnetic field

Three-dimensional numerical simulation of electromagnetic fields by the VFEM yields a solution of the forward problem in the entire computational domain. This makes it possible to study the behavior of the electric-field intensity with time and the behavior of the eddy current density and charges on the surfaces of the contacts between areas of different conductivities.

In model 1, the dipping boundary separates two areas of contrasting resistivities (by 20 times). The current toroid begins to spread in the right subarea with a resistivity of 200 Ohm·m. The distribution of eddy currents till 70 μs is the same as in a homogeneous half-space. By 70 μs, the current toroid, consisting of eddy currents parallel to the day surface, reaches the dipping boundary and a redistribution of the currents begins in the medium.

The dipping plane is an interfragmental boundary between two contrasting media at which the tangential components of the fields and the normal components of the currents should be continuous. The current toroid has two nonzero components: J_x and J_y, oriented parallel to the $0x$ and $0y$ axes. The electric-field intensity also has two components, because it is related to current through Ohm's law $\mathbf{J} = \sigma\mathbf{E}$.

The normal component of the current density should be continuous at the interfragmental boundaries. Correspondingly, the normal component of the electric-field intensity jumps proportionally to the conductivity ratio of the media.

Table 2. Maximum relative EMF deviation (%) for approximated models

Maximum relative EMF deviation	4	8	16	32	64
$\max(\lVert E - E_N\rVert / \lVert E\rVert)$	34	30	11	4	1.4

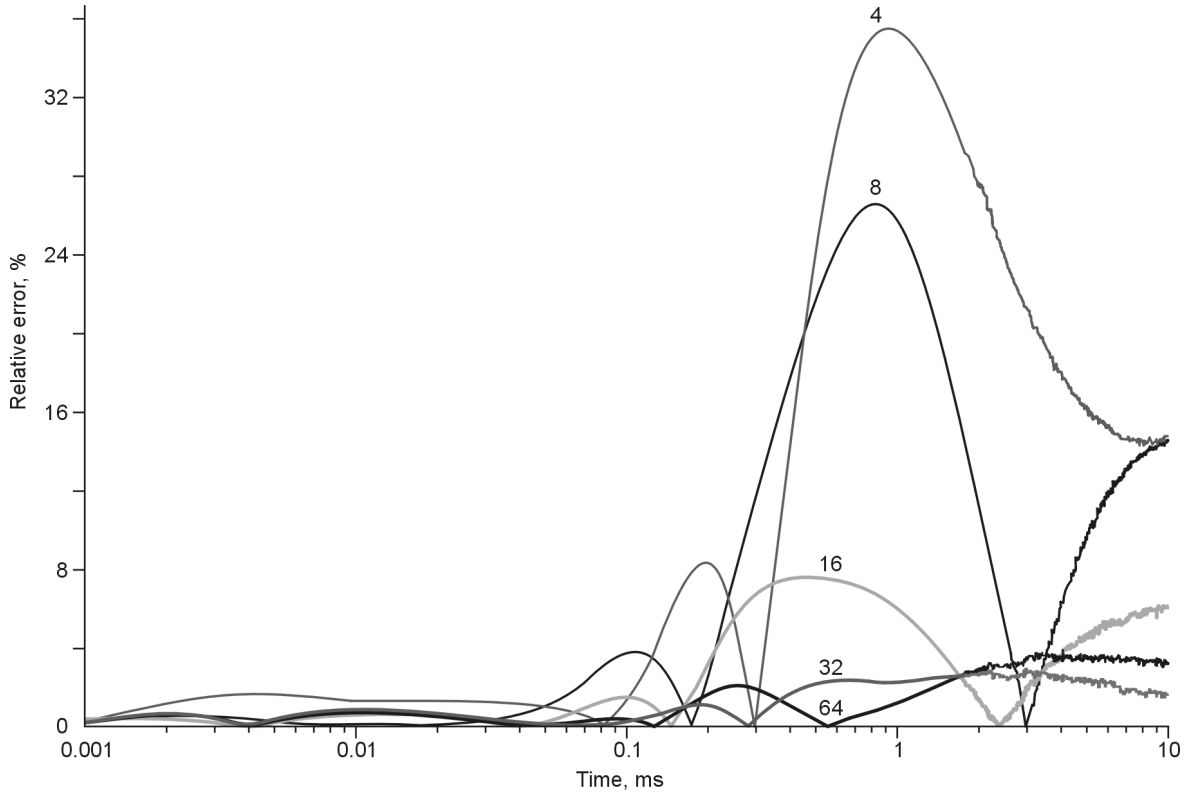

Fig. 3. Relative error of the EMF (V) of the form $\left|E(t)-\tilde{E}(t)\right| / \left|E(t)\right|$ vs. time (s). $E(t)$, EMF for a model with a dipping boundary; $\tilde{E}(t)$, EMF curves for models with a boundary approximated by $2N$ segments. $2N$, cipher of the curves.

The continuity of the normal current component on the inclined surface is ensured by the surface charges at the boundary, which change the electric-field intensity and the configuration of the currents in the medium. Near the dipping boundary, a third component of the electric field E_z appears under the effect of induced surface charges, which forms the normal field component $\mathbf{E}^n = \mathbf{E} \times \mathbf{n}$ together with E_x.

As the current toroid approaches the boundary, its isosurfaces change their configuration. In a homogeneous medium, all the current-density isosurfaces are toroids of different thicknesses with a single center. As the electric field interacts with the dipping plane, the current isosurfaces transform into a structure combining a toroid and an isosurface localized on the dipping-surface plane (Fig. 4). Within 0.1–0.2 ms, the current values are redistributed between the toroid and the isosurfaces on the boundary plane (Fig. 5).

By 0.70 ms, the currents in the right subarea (resistivity 200 Ohm·m) completely cross the boundary into an area with a resistivity of 10 Ohm·m, forming a new system of currents near the interfragmental boundary. The latter is asymmetric and extends along the inclined plane. The peak currents are concentrated in the upper part of the current bundle, and their isosurfaces take on the shape of a crescent with ends down. Isosurfaces with lower values but larger surface area are closed, and their center is localized at a depth of 350–400 m. The newly formed current bundle of the new configuration spreads in the left subarea parallel to the dipping plane (Fig. 6).

Model 2 (Fig. 1*b*) has two dipping boundaries (boundary *1* is the same as in model 1). The plane boundary *2* is perpendicular to boundary *1*. The subarea to the right of boundary *1* will be called right. The part of the area limited by boundaries *1* and *2* will be called middle, and the remaining part of the medium to the left of boundaries *1* and *2* will be called left. The resistivity contrast at boundary *2* equals 2 (resistivity of the middle area is 5 Ohm·m) or 100 (resistivity of the middle area is 100 Ohm·m). The resistivity contrast at boundary *1* is 20 to a depth of 500 m and 2 or 100 at depths greater than 500 m, depending on the middle-area resistivity.

The current vortex begins to spread in model 2 similarly to that in model 1, i.e., approaches boundary *1*, interacts with it, and changes its configuration during the transition to the left subarea. The subsequent behavior of the currents depends on the middle-area resistivity. If the middle area has a high conductivity, the currents formed near the upper part of boundary *1* partly flow into the middle area and spread therein, predominantly stretching along boundary *1*. In low-resistivity areas (5 Ohm·m), the current distribution has a low velocity, whereas the current-attenuation rate is high.

The maximum concentration of charges at boundary *1* (~2 mC/m^2) as the current bundle passes from right to left subarea. As the currents pass to the left subarea, the charges tend to attenuate and spread downward on the boundary plane.

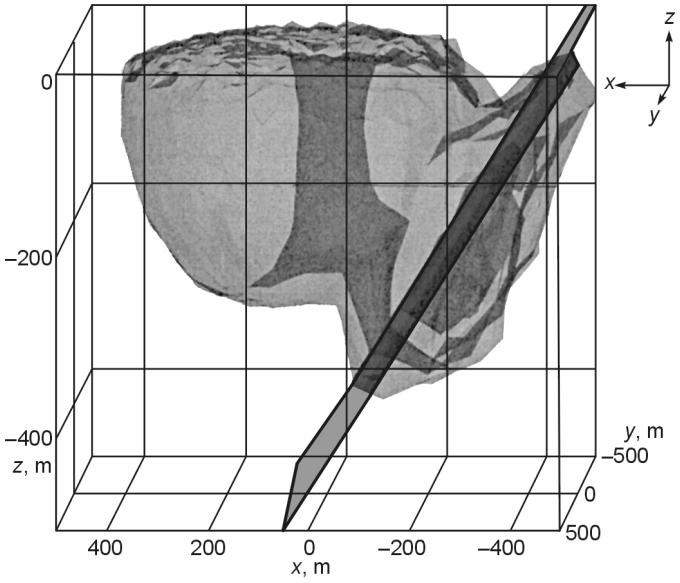

Fig. 4. Shape of the maximum current isosurface for model 1 near the dipping boundary at the moment 0.1 ms.

A small number of charges at boundary *2* (~10 μC/m^2) are concentrated near the intersection of boundaries *1* and *2* within 0.1–0.7 ms. The currents in the middle area later attenuate and move away from boundary *2*, but the peak current approaches the boundary from the left area and charges of ~3 μC/m^2 spread to depths of 800–900 m.

When the middle area has a high resistivity (1000 Ohm·m), the lower part of the current in the left area changes the direction of its spread rather than penetrates the middle area. The lower part of the current bundle moves to the left along boundary *2*. The peak current, concentrated in the upper part of the current ring, expands in the left area toward the outer boundary. The current isosurfaces in the middle of the computational domain replicates the shape of boundaries *1* and *2*, which limit the current.

The distribution of the induced charges at boundary *2* (two opposite charge poles spread along the plane of boundary *2*) is typical of current–dipping plane interaction. Starting from 0.3 ms, the intersection of boundaries *1* and *2* is detectable at boundary *1*. The induced charges, concentrated above the intersection, are partly compensated for by opposite charges in a small neighboring area below the intersection of boundaries *1* and *2*.

Model 3 (Fig. 1*c*) differs from model 2 in the shallower depth (dipping) of the intersection of boundaries *1* and *2* (100 m). However, this causes a dramatic change in the behavior of the field and currents. Expanding at early times (till 0.1 ms), the current bundle immediately appears at the intersection of three media of different resistivities: the right area with the peak current (200 Ohm·m), left area (10 Ohm·m), and middle area (5 or 1000 Ohm·m).

If the middle area has a low resistivity, the currents select the area with the lowest resistivity; i.e., the peak current completely passes into the middle area. The shape of the currents is similar to the current bundle in the left area in model 1. The current bundle later expands in the middle area between boundaries *1* and *2*. The current, which is mainly parallel to boundary *1*, expands along and below the boundary. The peak current is distorted as it closely approaches boundary *2* and expands along and below the boundary.

The currents in the high-resistivity middle area show opposite behavior. The peak current completely passes into the left area and spreads only therein. The current bundle takes on the angular shape of the left subarea, closely approaching the inner boundaries *1* and *2* from the left. Induced charges form at boundary *1* only to a depth of 100 m, i.e., in the area with less contrasting resistivity. The charge distribution at boundary *2* corresponds to a common distribution on a dipping plane.

The dipping plane in model 4 crosses a layered medium of complicated configuration (Fig. 1*d*). The resistivity contrast along the dipping plane to a depth of 250 m is 40 times (5 and 200 Ohm·m) or five times (1000 and 200 Ohm·m). Within 250–500 m to the right and to the left of the dipping plane, the resistivity is 200 Ohm·m, i.e., noncontrasting. The resistivity contrast from 500 to 750 m below the day surface is 20 times (200 and 10 Ohm·m). Great depths show no contrast, because the dipping plane passes within the underlying homogeneous layer.

The current toroid expands very slowly in the conducting upper layer (5 Ohm·m) with gradual attenuation. It interacts with the dipping boundary only 3 ms after the current switch-off. The left part of the current toroid bumps into the dipping boundary, and the peak current is redistributed closer to the boundary. The right part of the toroid spreads within the conducting layer, gradually extending to the outer boundaries of the area. Note the slight downward tendency of the current toroid. The current bundle without a vertical component neither produces charges at the horizontal boundary between the first and second layers of the medium nor tries to cross this boundary.

The current–dipping plane interaction produces two groups of opposite charges above the intersection (250 m) of the dipping plane and the horizontal boundary between the first

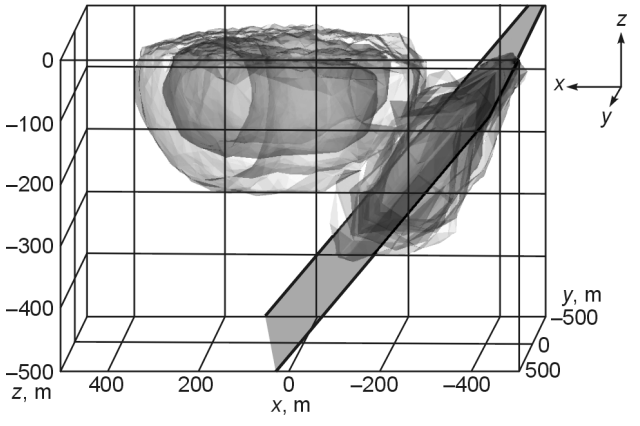

Fig. 5. Shape of several embedded current isosurfaces (30–50 μA) for model 1 near the dipping boundary at the moment 0.2 ms.

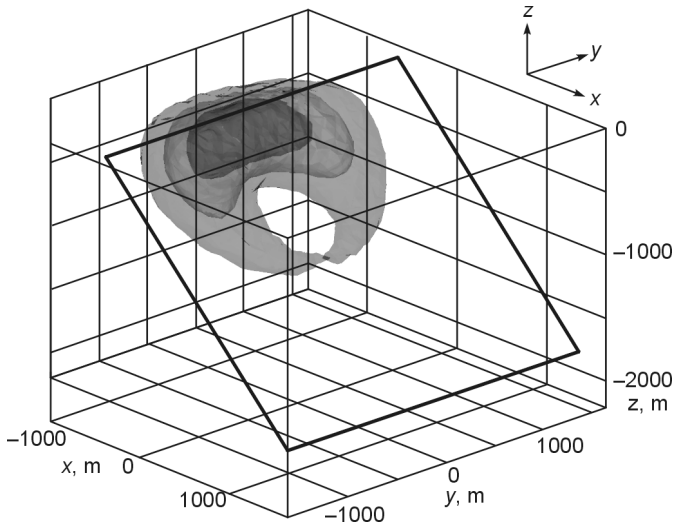

Fig. 6. Shape of several embedded current isosurfaces (0.3–0.5 μA) for model 1 at the moment 10 ms.

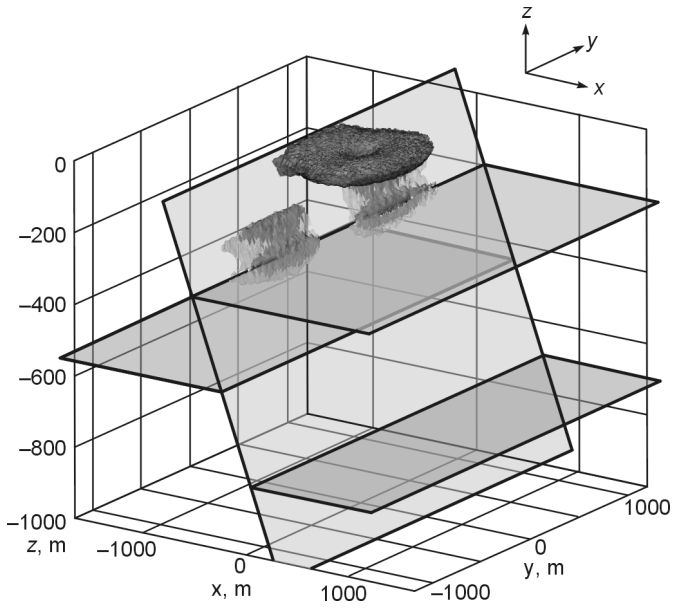

Fig. 7. Shape of several embedded current isosurfaces (0.3–0.5 μA) for model 4 at the moment 5 ms.

and second layers of the medium (Fig. 7). The vertical current component J_z, which replicates the shape of the induced charges, appears in this part of the dipping boundary. As compared with model 1, in which the right part of the current toroid turned toward the dipping boundary and closed the system of currents, the right part of the currents in model 4 completely attenuates without leaving the first layer. The currents in the second layer fail to form a closed system over the modeling period. The isosurfaces of the currents are paraboloids flowing from the dipping plane, whose upper part replicates the upper boundary of the second layer (combination of the horizontal boundary and the upper part of the dipping plane). This shape of the currents is due to the predominance of two current components, J_x and J_z. The current component J_y, tangent to the dipping plane, passes into the second layer and attenuates therein at the penetration depth.

The distribution of the induced charges corresponds to that of the contrasts along the dipping plane. The induced charges accumulate above the intersection of the first horizontal boundary with the dipping plane at a depth of 250 m. At late times (more than 13 ms), the intersection of the dipping plane with the second horizontal boundary (500 m) is slightly lit from the bottom by the induced charges. The value of the charges is ~0.3 μC/m^2.

The current bundle for the high-resistivity first layer spreads fast, so that the left part of the bundle touches the dipping plane already at very early times (20–30 μs). The current does not manage to attenuate and penetrates far through the dipping boundary (~100 m). The shape of the current resembles the left part of the current bundle, which is located to the left of the boundary and bumps into it. Within 0.1–0.3 ms, the currents shift gradually down the dipping plane with simultaneous attenuation of the horizontal part of the currents, which replicate the shape of the initial toroid. The subsequent behavior of the currents is similar, but the absolute values of the current are higher owing to its fast penetration into the area with a resistivity of 200 Ohm·m and it spreads farther within the simulation area.

This is evident from the distribution of the induced charges. The induction is carried out in two parts of the dipping plane: at depths of 0–250 and 500–750 m. The charges are redistributed with time, first to a depth of 250 m, and then charges appear and spread between the horizons z = –500 m and z = –750 m (Fig. 8).

Inversion of the data obtained in the models with dipping boundaries

Transient EMF curves are mostly interpreted within layered homogeneous models with plane-parallel boundaries, because these models possess the best developed set of programs and algorithms for quantitative inversion of the data. As pointed out above, eddy currents serve as signal sources in this case, whereas the part connected with charges does not exist. As these sources are important in media with dipping boundaries, inversion within a horizontally layered model will not yield a realistic spatial distribution of resistivities because of considerable inconsistency between the model data and the interpretation technique.

Transient EMF curves obtained on the profile intersecting the dipping boundary at a right angle were used as the initial data (model 1). The inversion was conducted in the TEM-IP software (Antonov and Orlovskaya, 2010; Antonov et al., 2010, 2011; Shein et al., 2012; Shtabel' and Antonov, 2011). Figure 9 shows a geoelectric section obtained from the inversion of the model data calculated for the profile which crosses the areas separated by the dipping boundary. Along with considerable resistivity differences detected by 1D inver-

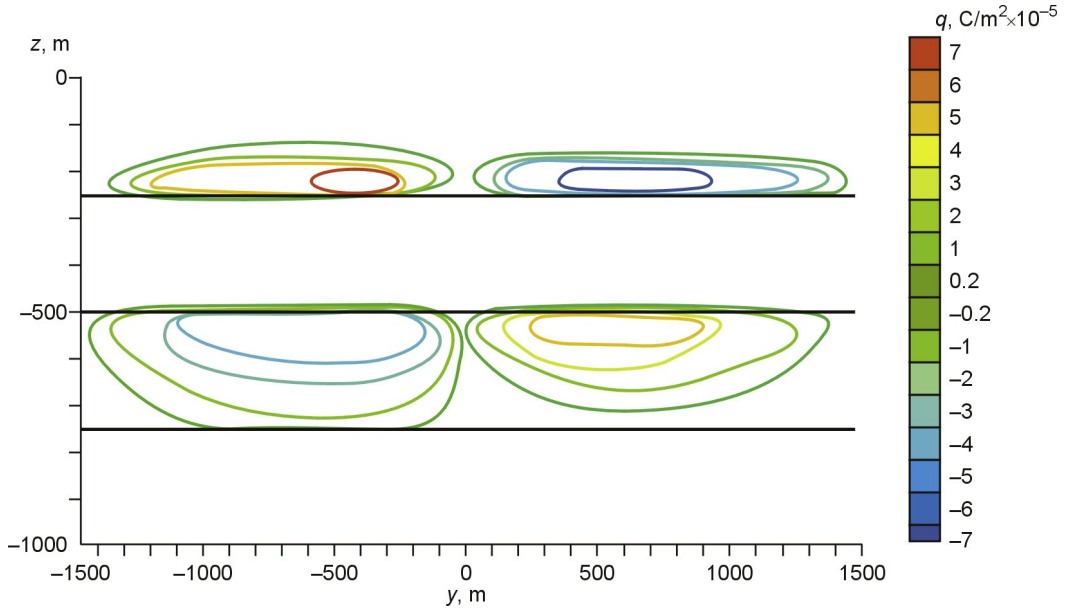

Fig. 8. Distribution of the charges along the dipping plane at the moment 0.63 ms for model 4.

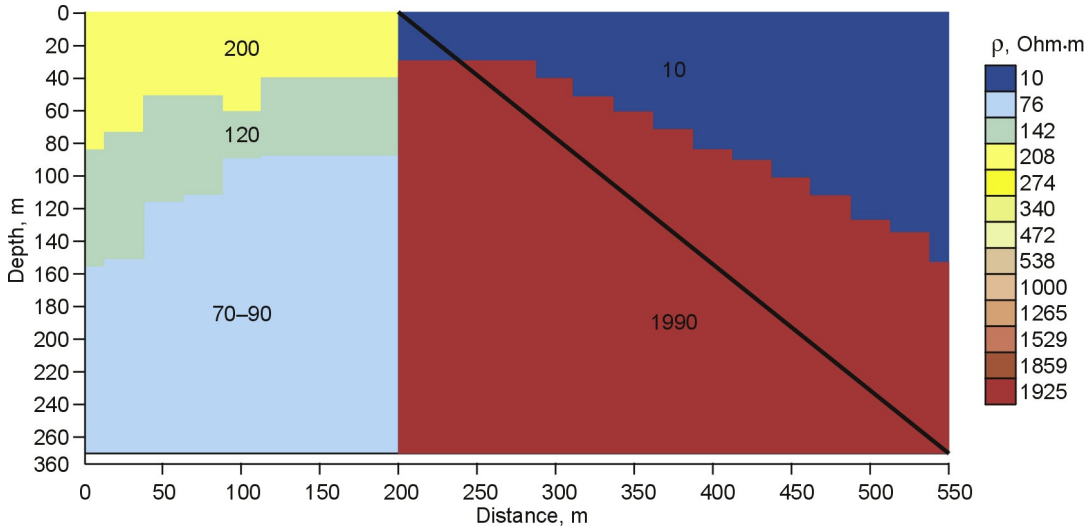

Fig. 9. Geoelectric section from inversion within a model for a horizontally layered medium.

sion, we get a wrong idea of the localization of the dipping boundary.

Conclusions

The studies show that, if near-vertical boundaries are approximated by few rectangular blocks (fewer than ten), the error in EMF curves obtained from the solution of a forward problem is too high for these curves to be used in the solution of an inverse problem. On the other hand, models constructed with regard to the minimum deviation of EMF curves do not correspond to the initial model for the medium. The application of block structures in models used for solving inverse problems is justified only with a large number of small blocks. It is incorrect to select a model with blocks whose dimensions are close to those of the coil and domain, because this selection yields a model without any common points with the actual section. The solution of inverse problems should be based on that of a forward problem in areas with curved boundaries as a 3D problem with regard to all the factors affecting the electromagnetic field.

The study was supported by the Ministry of Education and Science of the Russian Federation, Agreement no. 14.V37.21.0615 "Development and Application of Efficient Programs and Algorithms for Modeling Nonstationary Electromagnetic Fields in Three-Dimensional Conducting and Polarizing Geologic Media."

References

Antonov, E.Yu., Orlovskaya, N.V., 2010. Numerical simulation of pulsed soundings of conducting near-vertical inhomogeneities [electronic resource], in: Int. Sci. Conf. "Electromagnetic Methods-2010" (Irkutsk, 15–20 August 2010) [in Russian]. CD-ROM, ISBN 978-5-88942-096-5.

Antonov, E.Yu., Kozhevnikov, N.O., Korsakov, M.A., 2010. TEM-IP—interpretation software for transient inductive EM data with respect to induced polarization [electronic resource], in: Int. Sci. Conf. "Electromagnetic Methods-2010" (Irkutsk, 15–20 August 2010) [in Russian]. CD-ROM, ISBN 978-5-88942-096-5.

Antonov, E.Yu., Shtabel', N.V., Korsakov, M.A., 2011. Numerical simulation and inversion of data from pulsed soundings of complicated geologic media, in: Erofeev, L.Ya., Isaev, V.I. (Eds.), Geophysical Methods in Prospecting [in Russian]. Izd. Tomsk. Politekh. Univ., Tomsk, pp. 8–11.

Epov, M.I., Sukhorukova, K.V., Antonov, E.Yu., 1994. Kinematics of the nonstationary electromagnetic field in layered conducting media, in: Theory and Practice of Magnetotelluric Soundings, Proc. Conf. (Moscow, 20–23 December 1994) [in Russian]. Moscow, pp. 11–12.

Epov, M.I., Shurina, E.P., Shtabel, N.V., 2012. Features of 3D electromagnetic fields modeling for geoelectric problems, in: ACE2012—7th Workshop on Advanced Computational Electromagnetics 29.02.–02.03.2012, Karlsruhe Inst. of Technology (KIT), Karlsruhe, electronic resource, http://ace2012.math.kit.edu/abstracts/shtabel_epov_shurina.pdf.

Nabighian, M.N., 1979. Quasi-static transient response of a conducting half-space: An approximate representation. Geophysics 44 (10), 1700–1705.

Nédélec, J.-C., 1980. Mixed finite elements in R^3. Numerische Mathematik 35 (3), 315–341.

Nédélec, J.-C., 1986. A new family of mixed finite elements in R^3. Numerische Mathematik 50 (1), 57–81.

Shein, A.N., Antonov, E.Yu., Kremer, I.A., Ivanov, M.I., 2012. Interpretation TEM-data by the program Modem3D for 3D modeling of transient electromagnetic field, in: The 6th Int. Siberian Early Career GeoScientists Conf.: Proc. of the Conf. (Novosibirsk, 9–23 June 2012). IGM and IPPG SB RAS, NSU, Novosibirsk, pp. 303–304.

Shtabel', N.V., Antonov, E.Yu., 2011. Numerical simulation of the forward problem of pulsed soundings in areas with near-vertical inhomogeneities, in: Proc. of the Fifth All-Russ. Workshop, Named after M.N. Berdichevskii and L.L. Van'yan, on Electromagnetic Soundings of the Earth—EMS-2011 [in Russian]. Sankt-Peterburgsk. Gos. Univ., St. Petersburg, Book 2, pp. 142–145.

Tamm, I.E., 1976. Fundamentals of the Theory of Electricity: A Handbook, 9th ed. [in Russian]. Nauka, Moscow.

Editorial responsibility: A.D. Duchkov